Pergamon

Int. J. Heat Mass Transfer. Vol. 40, No. 13, pp. 3079–3088, 1997

Printed in Great Britain
0017–9310/97 \$17.00+0.00

PII: S0017–9310(96)00356–0

# Heat transfer and fluid flow in microchannels

G. MOHIUDDIN MALA, DONGQING LI† and J. D. DALE

Department of Mechanical Engineering, University of Alberta, Edmonton, Alberta, Canada T6G 2G8

(*Received* 14 *May* 1996 *and in final form* 15 *October* 1996)

**Abstract**—This paper investigates the effects of the EDL at the solid–liquid interface on liquid flow and heat transfer through a microchannel between two parallel plates at constant and equal temperatures. A linear approximate solution of the Poisson–Boltzmann equation is used to describe the EDL field near the solid–liquid interface. The electrical body force resulting from the double layer field is considered in the equation of motion. The equation of motion is solved for the steady state flow. Effects of the EDL field and the channel size on the velocity distribution, streaming potential, apparent viscosity, temperature distribution and heat transfer coefficient are discussed in this paper. © 1997 Elsevier Science Ltd.

## INTRODUCTION

A variety of high-density, high-power and high-speed microelectronic devices require high rates of heat removal. The rate of heat dissipation is expected to be of the order of 100 W cm$^{-2}$ [1]. To operate the electronic device at an optimum temperature, it is necessary to develop efficient heat removal methods. One such method is to use the microchannel heat sinks. A microchannel heat sink is a structure with many microscale channels of large aspect ratios built on the back of the microchip. A liquid is forced through these microchannels to carry away the energy.

The concept of the microchannel heat sinks was introduced by Tuckerman and Pease [2]. A detailed review of several other research works on microchannel heat sinks can be found elsewhere [3]. To design an effective heat sink it is necessary to understand the flow characteristics in microchannels. Only after obtaining the velocity distribution can the energy equation be solved to determine the heat transfer characteristics. However, conventional transport theories cannot explain many phenomena associated with the microscale flow. For example, Eringen [4] proposed a theory which states that fluid flow in micro-channels will deviate from that predicted by Navier–Stokes equations. Pfahler [5] measured the friction coefficient in microchannels and found a significantly higher flow rate than expected for both isopropanol and silicon oil. His results indicate that polar nature of the fluid may play a role in the change in the observed viscosity. Choi *et al.* [6] measured friction factor in microtubes of inside diameters 3–81 $\mu$m using nitrogen gas. They found that for diameters smaller than 10 $\mu$m, the friction factor constant $C_f = 53$, instead of 64. Harley and Bau [7] measured the friction factor in channels of trapezoidal and square cross-sections. They found experimentally that $C_f$ ranged from 49 for the square channels to 512 for the trapezoidal channels. Peng *et al.* [8] found experimentally that transition to turbulent flow began at $Re = 200$–700, and that fully turbulent connective heat transfer was reached at $Re = 400$–1500. They also observed that transitional $Re$ diminished as the size of the microchannel decreased. Wang and Peng [9] concluded that these effects were due to large changes in the thermophysical properties of the liquid due to high heat fluxes in small channels.

One possible explanation for these observed effects is that they are largely due to the interfacial effects such as interfacial electric double layer (EDL). These interfacial effects are ignored in macroscale fluid mechanics. However most solid surfaces have electrostatic charges i.e. an electrical surface potential. If the liquid contains very small amounts of ions, the electrostatic charges on the solid surface will attract the counterions in the liquid to establish an electrical field. The arrangement of the electrostatic charges on the solid surface and the balancing charges in the liquid is called the EDL, as illustrated in Fig. 1 [10]. Because of the electrical field, the ionic concentration near the solid surface is higher than that in the bulk liquid. In compact layer, which is about 0.5 nm thick, the ions are strongly attracted to the wall surface and are immobile. In diffuse double layer the ions are affected less by the electrical field and are mobile. The thickness of the diffuse EDL ranges from a few nanometers up to several hundreds of nanometers, depending on the electric potential of the solid surface, the bulk ionic concentration and other properties of the liquid.

When a liquid is forced through a microchannel under hydrostatic pressure, the ions in the mobile part of the EDL are carried towards one end. This causes

† Author to whom correspondence should be addressed.

## NOMENCLATURE

| | |
|---|---|
| $A_c$ | cross-sectional area of the flow channel |
| $Br$ | Brinkman number |
| $C_f$ | friction constant |
| EDL | electric double layer |
| $Ec$ | Eckert number |
| $E_s$ | streaming potential |
| $E_z$ | electric field strength |
| $G_1$ | non-dimensional parameter |
| $G_2$ | non-dimensional parameter |
| $G_3$ | non-dimensional parameter |
| $I_c$, $I_s$ | conduction and streaming currents, respectively |
| $Nu$ | Nusselt number |
| $Nu_{av}$ | average Nusselt number |
| $P_z$ | pressure gradient in $z$-direction $= -\mathrm{d}p/\mathrm{d}Z$ |
| $Q$ | volume flow rate through the channel |
| $Q_p$ | conventional volume flow rate through the channel |
| $Re$ | Reynolds number |
| $T$ | absolute temperature |
| $T_i$ | inlet fluid temperature |
| $T_m$ | mean temperature of the fluid |
| $T_w$ | wall temperature |
| $V_{av}$ | average velocity of the fluid |
| $V_{max}$ | maximum velocity of the fluid |
| $V_0$ | reference velocity |
| $V_z$ | velocity of the fluid in $z$-direction |
| $X$ | $x$ co-ordinate |
| $Z$ | $z$ co-ordinate |
| $a$ | half distance between the plates |
| $c_p$ | specific heat of the fluid |
| $e$ | electron charge, $1.6021 \times 10^{-19}$ C |
| $f$ | friction factor |
| $h$ | heat transfer coefficient |
| $k$ | Debye–Huckel parameter [m$^{-1}$] |
| $k_b$ | Boltzmann constant, $1.3805 \times 10^{-23}$ J mol$^{-1}$ K$^{-1}$ |
| $k_f$ | thermal conductivity of the fluid |
| $l$ | length of the channel |
| $n^+$, $n^-$ | concentration of positive and negative ions [m$^{-3}$] |
| $n_0$ | average number of positive or negative ions/unit volume or ionic number concentration |
| $z^+$, $z^-$ | valence of the positive and negative ions. |

Greek symbols

| | |
|---|---|
| $\alpha_t$ | thermal diffusivity of the fluid |
| $\varepsilon$ | dielectric constant of the medium, dimensionless |
| $\varepsilon_0$ | permittivity of vacuum, $8.854 \times 10^{-12}$ C V$^{-1}$ m$^{-1}$ |
| $\kappa$ | non-dimensional electrokinetic separation distance between the two plates |
| $\lambda_0$ | electrical conductivity of the fluid [($\Omega$ m)$^{-1}$] |
| $\mu$ | dynamic viscosity of the fluid |
| $\mu_a$ | apparent viscosity of the fluid |
| $\theta$ | non-dimensional temperature distribution |
| $\theta_m$ | non-dimensional mean temperature distribution |
| $\rho$ | charge density [C m$^{-3}$] |
| $\rho_f$ | density of fluid |
| $\tau_w$ | shear stress at the channel wall |
| $\xi$ | zeta potential, i.e. the electric potential at the boundary between the diffuse double layer and the compact layer |
| $\psi$ | electrostatic potential at any point in the electric double layer |
| $\psi_0$ | electrostatic potential at the channel wall. |

Superscript

| | |
|---|---|
| — | non-dimensional parameters. |

an electrical current, called streaming current, to flow in the direction of the liquid flow. The accumulation of ions downstream sets up an electrical field with an electrical potential called the streaming potential. This field causes a current, called conduction current, to flow back in the opposite direction. When conduction current is equal to the streaming current a steady state is reached. It is easy to understand that, when the ions are moved in the diffuse double layer, they pull the liquid along with them. However, the motion of the ions in the diffuse double layer is subject to the electrical potential of the double layer. Thus the liquid flow and associated heat transfer are affected by the presence of the EDL.

In macroscale flow, these interfacial electrokinetic effects are negligible as the thickness of the EDL is negligible compared to the hydraulic radius of the flow channel. However, in microscale flow the EDL thickness is comparable to the hydraulic radius of the flow channel. For submicron capillaries the EDL thickness may be even larger than the radius of the capillary. Thus EDL effects must be considered in the studies of microscale flow and heat transfer. There are few analytical studies in literature which account for these effects on flow characteristics. Rice and Whitehead [11] studied the effect of the surface potential on liquid transport through narrow cylindrical capillaries with the Debye–Huckel approximation to the surface potential distribution. Levine *et al.* [12] extended the Rice and Whitehead model to higher zeta potential by

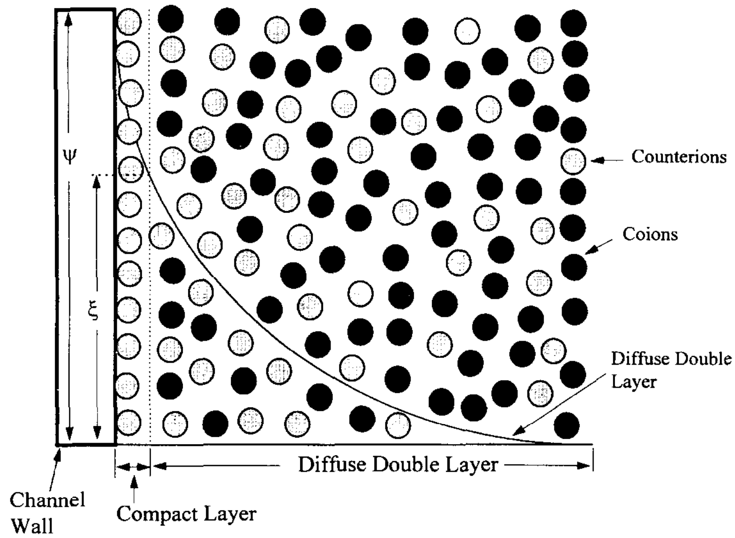


Fig. 1. Schematic representation of the electrical double layer at the channel wall.

developing an analytical approximation to the solution of the Poisson–Boltzmann equation.

## POISSON–BOLTZMANN EQUATION

Consider a fluid phase of infinite dilution containing positive and negative ions in contact with a planar positively charged surface. The surface bears a uniform electrostatic potential $\psi_0$, which decreases as one proceeds out into the fluid, as shown in Fig. 1. Far away from the wall, the concentration of the positive and negative ions is equal. The electrostatic potential $\psi$, at any point near the surface is related to the net number of electrical charges per unit volume $\rho$, in the neighborhood of the point, which measures the excess of the positive ions over negative ions or vice versa. According to the theory of electrostatics, the relation between $\psi$ and $\rho$ is given by the Poisson's equation, which for a flat surface is

$$\frac{d^2\psi}{dX^2} = -\frac{\rho}{\varepsilon_0\varepsilon}. \quad (1)$$

The probability of finding an ion at some particular point will be proportional to the Boltzmann factor $e^{-ze\psi/k_bT}$. For the case of any fluid consisting of two kinds of ions of equal and opposite charge $z^+$, $z^-$, the number of ions of each type are given by the Boltzmann equation

$$n^- = n_0 e^{ze\psi/k_bT} \quad \text{and} \quad n^+ = n_0 e^{-ze\psi/k_bT}.$$

The net charge density in a unit volume of the fluid is given by

$$\rho = (n^+ - n^-)ze = -2n_0 ze \sinh(ze\psi/k_bT). \quad (2)$$

Substituting equation (2) in equation (1), a nonlinear second-order one dimensional equation known as Poisson–Boltzmann equation is obtained.

$$\frac{d^2\psi}{dX^2} = \frac{2n_0 ze}{\varepsilon_0\varepsilon}\sinh\left(\frac{ze\psi}{k_bT}\right). \quad (3)$$

Non-dimensionalizing the above equation via

$$\bar{X} = \frac{X}{a} \quad \bar{\psi} = \frac{ze\psi}{k_bT} \quad \text{and} \quad \bar{\rho}(\bar{X}) = \frac{\rho(X)}{n_0 ze} \quad (4)$$

a non-dimensional form of equation (1) and equation (3), after some simplification is

$$\frac{d^2\bar{\psi}}{d\bar{X}^2} = -\frac{\kappa^2}{2}\bar{\rho}(\bar{X}) \quad (5)$$

$$\frac{d^2\bar{\psi}}{d\bar{X}^2} = \kappa^2\sinh(\bar{\psi}) \quad (6)$$

where $k = (2n_0 z^2 e^2/\varepsilon\varepsilon_0 k_b T)^{1/2}$ and $(a * k) = \kappa$. The quantity '$k$' is called the Debye–Huckel parameter, while '$1/k$' is referred to as the characteristic thickness of EDL.

## SOLUTION OF THE POISSON–BOLTZMANN EQUATION

If the electrical potential is small compared to the thermal energy of the ions, i.e. ($|ze\psi| < |k_bT|$) so that the exponential in equation (6) can be approximated by the first terms in a Taylor series. This transforms equation (6) to

$$\frac{d^2\bar{\psi}}{d\bar{X}^2} = \kappa^2\bar{\psi}. \quad (7)$$

In literature this is called the Debye–Huckle linear approximation. The solution of the above equation can easily be obtained. Consider a flow channel

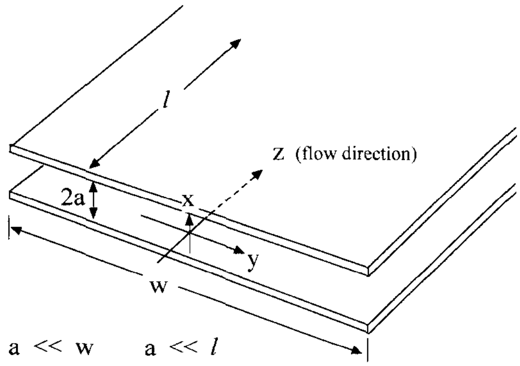


Fig. 2. Microchannel between two parallel plates.

between two parallel plates as shown in Fig. 2. If the electrical potential of the channel surface is small and the separation distance between the two plates is larger than the thickness of the EDL so that the EDLs near the two plates will not overlap, the appropriate boundary conditions are: at $\bar{X} = 0$, $\bar{\psi} \approx 0$ and at $\bar{X} \approx \pm 1$, $\bar{\psi} = \bar{\xi} = (ze\xi/k_b T)$. With these boundary conditions the solution is

$$\bar{\psi} = \frac{\bar{\xi}}{\sinh(\kappa)} |\sinh(\kappa\bar{X})|. \tag{8}$$

## EQUATION OF MOTION

Consider a one-dimensional fully developed laminar flow through two parallel plates of unit width as shown in Fig. 2. The forces acting on an element of fluid include the pressure force, the viscous force and the electric body force generated by the double layer electric field. The equation of motion is the $Z$-directional momentum equation.

$$\mu \frac{d^2 V_z}{dX^2} - \frac{dp}{dZ} + E_z \rho(x) = 0 \tag{9}$$

where $E_z \rho(x)$ is the electrical body force. To non-dimensionalize equation (9) use $\bar{E}_s = E_s/\xi$, $\bar{V}_z = V_z/V_0$ and replacing $\bar{\rho}(\bar{X})$ from equation (5), we obtain

$$\frac{d^2 \bar{V}_z}{d\bar{X}^2} + G_1 - \frac{2G_2 \bar{E}_s}{\kappa^2} \frac{d^2 \bar{\psi}}{d\bar{X}^2} = 0 \tag{10}$$

where the two non-dimensional numbers are

$$G_1 = \frac{a^2 P_z}{\mu V_0} \quad \text{and} \quad G_2 = \frac{\xi n_0 z e a^2}{l \mu V_0}.$$

Note, $E_z = E_s/l$ and let $P_z = -dp/dZ$. Integrating equation (10) twice we get

$$\bar{V}_z + \frac{G_1 \bar{X}^2}{2} - \frac{2G_2 \bar{E}_s}{\kappa^2} \bar{\psi} = C_1 \bar{X} + C_2.$$

The constants of integration $C_1$ and $C_2$ can be found by employing the appropriate boundary conditions, namely at $\bar{X} = \pm 1$, $\bar{V}_z = 0$, $\bar{\psi} = \bar{\xi}$. After evaluating the constants $C_1$ and $C_2$ and substituting for $\bar{\psi}$ from equation (8) the non-dimensional velocity distribution is

$$\bar{V}_z = \frac{G_1}{2}(1 - \bar{X}^2) - \frac{2G_2 \bar{E}_s \bar{\xi}}{\kappa^2} \left\{ 1 - \left| \frac{\sinh(\kappa\bar{X})}{\sinh(\kappa)} \right| \right\}. \tag{11}$$

## THE STREAMING POTENTIAL

As seen from equation (11), the velocity distribution can be calculated only if the streaming potential $\bar{E}_s$ is known. As explained previously, in absence of an applied electric field when a liquid is forced through a channel under hydrostatic pressure an electrical field is generated. The potential of this electrical field is called the streaming potential. The current due to the transport of charges by the liquid flow, called streaming current, is given by

$$I_s = \int_{A_c} V_z \rho(X) \, dA_c. \tag{12}$$

After non-dimensionalizing $V_z$ and $\rho(X)$ and substituting for $\bar{\rho}(\bar{X})$ from equation (2), making use of the linear approximation, the nondimensional streaming current becomes

$$\bar{I}_s = \frac{I_s}{2V_0 n_0 z e a} = -2 \int_0^1 \bar{V}_z \bar{\psi} \, d\bar{X}. \tag{13}$$

Substituting $\bar{V}_z$ from equation (11) and $\bar{\psi}$ from equation (8), we obtain

$$\bar{I}_s = -2\alpha \left[ \frac{G_1}{2} \{ I_1 - I_2 \} - \frac{2G_2 \bar{E}_s \bar{\xi}}{\kappa^2} I_3 + \frac{2G_2 \bar{E}_s \bar{\xi}}{\kappa^2 \sinh(\kappa)} I_4 \right] \tag{14}$$

where $\alpha = \bar{\xi}/\sinh(\kappa)$.

$$I_1 = I_3 = \int_0^1 \sinh(\kappa\bar{X}) \, d\bar{X} = \frac{\cosh(\kappa) - 1}{\kappa}$$

$$I_2 = \int_0^1 \bar{X}^2 \sinh(\kappa\bar{X}) \, d\bar{X} = \left( \frac{1}{\kappa} + \frac{2}{\kappa} \right) \cosh(\kappa) - \frac{2}{\kappa^2} \sinh(\kappa) - \frac{2}{\kappa^3}$$

$$I_4 = \int_0^1 \frac{\sinh^2(\kappa\bar{X})}{\sinh(\kappa)} \, d\bar{X} = \frac{\sinh(\kappa)\cosh(\kappa)}{2\kappa} - \frac{1}{2}.$$

The streaming potential generated by the streaming current will produce a conduction current in the reverse direction and is given by

$$I_c = \frac{E_s \lambda_0 A_c}{l}. \tag{15}$$

The electrical condutivity, $\lambda_0$ is assumed to be constant. Non-dimensionalizing as before with $\bar{l} = l/a$, the non-dimensional conduction current is given by

$$\bar{I}_c = \frac{I_c}{\xi a \lambda_0} = \frac{\bar{E}_s \bar{A}_c}{\bar{l}}. \tag{16}$$

At a steady state, there will be no net current in the flow, i.e. $I_c + I_s = 0$. That is

$$\bar{I}_c + (V_0 n_0 zel/\xi\lambda_0)\bar{I}_s = 0.$$

Substituting for $\bar{I}_c$ and $\bar{I}_s$ from equations (16) and (14) the streaming potential is obtained as

$$\bar{E}_s = \frac{\alpha\kappa^2 G_1 G_3 (I_1 - I_2)}{\kappa^2 + 4G_3 G_2 \xi \alpha \{I_3 - I_4/\sinh(\kappa)\}} \tag{17}$$

where the nondimensional factor

$$G_3 = \frac{V_0 n_0 zel}{\xi \lambda_0}.$$

## VOLUME FLOW RATE

The volume flow rate through the parallel plates can be obtained by integrating the velocity distribution over the cross sectional area, as

$$Q = \int_{A_c} V_z \, dA_c. \tag{18}$$

In non-dimensional form, using equation (11) the result is

$$\bar{Q} = \frac{2G_1}{3} - \frac{4G_2 \bar{E}_s \xi}{\kappa^2} + \frac{4G_2 \bar{E}_s \xi}{\kappa^3} \frac{(\cosh(\kappa) - 1)}{\sinh(\kappa)}. \tag{19}$$

## THE ELECTROVISCOUS EFFECT

As discussed previously, the EDL field at the solid surface exerts electrical forces on the ions in the liquid, and hence restricts the motion of these ions. Consequently the presence of the EDL field will reduce the liquid flow in comparison with the cases of no EDL effects. For steady flow under an applied pressure gradient (in the absence of an externally applied electric field), the volume flow rate is given by equation (19). However, for flow between two parallel plates separated by a distance '$2a$' the volume flow rate can be written as

$$Q_p = \frac{2P_z a^3}{3\mu_a} \tag{20}$$

where $\mu_a$, apparent viscosity, is introduced to account for the EDL effects. If the EDL effect is negligible then $\mu_a = \mu$. Non-dimensionalizing the volume flow rate and rearranging yields

$$\bar{Q}_p = \frac{2G_1 \mu}{3\mu_a} \tag{21}$$

Equalizing equation (19) with equation (21), i.e. $\bar{Q} = \bar{Q}_p$, we obtain the ratio of the apparent viscosity to bulk viscosity.

$$\frac{\mu_a}{\mu} = \frac{\kappa^3 G_1}{\kappa^3 G_1 - 6G_2 \bar{E}_s \xi \kappa + 6G_2 \bar{E}_s \xi (\cosh(\kappa) - 1)/\sinh(\kappa)}. \tag{22}$$

## FRICTION CONSTANT

To calculate the friction constant, $C_f$, product of the friction factor and $Re$ the friction factor for flow between two parallel plates '$2a$' apart is given by

$$f = \frac{8\tau_w}{\rho_f V_{av}^2}$$

where

$$V_{av} = \frac{Q}{A_c}.$$

The shear stress is given by

$$\tau_w = \left|\mu \frac{dV_z}{dX}\right|_{X=\pm a} = \left|\frac{\mu V_0}{a} \frac{d\bar{V}_z}{d\bar{X}}\right|_{\bar{X}=\pm 1}.$$

Differentiating equation (11) once and substituting for $(d\bar{V}_z/d\bar{X})$, we obtain with $Re = (\rho_f V_{av} a/\mu)$ the friction constant $C_f$ as

$$C_f = fRe = \frac{8V_0}{V_{av}}\left(G_1 + \frac{2G_2 \bar{E}_s \xi}{\kappa} \coth(\kappa)\right). \tag{23}$$

## ENERGY EQUATION

Starting from the general form of the energy equation, performing an order of magnitude analysis to the fully developed flow in the microchannel yields equation (24).

$$\rho_f c_p \left(V_z \frac{\partial T}{\partial Z}\right) = k_f \left(\frac{\partial^2 T}{\partial X^2} + \frac{\partial^2 T}{\partial Z^2}\right) + \mu \left(\frac{\partial V_z}{\partial X}\right)^2 \tag{24}$$

with

$$\alpha_t = \frac{k_f}{c_p \rho_f} \quad \text{and} \quad Pr = \frac{\mu c_p}{k_f}$$

equation (24) reduces to

$$V_z \frac{\partial T}{\partial Z} = \alpha_t \left(\frac{\partial^2 T}{\partial X^2} + \frac{\partial^2 T}{\partial Z^2} + \frac{Pr}{c_p}\left(\frac{\partial V_z}{\partial X}\right)^2\right). \tag{25}$$

Non-dimensionalize equation (25) via

$$\bar{\alpha}_t = \frac{\alpha_t}{V_0 a}, \quad \bar{V}_z = \frac{V_z}{V_0}, \quad \bar{Z} = \frac{Z}{a},$$

$$\bar{X} = \frac{X}{a}, \quad \theta = \frac{T_w - T}{T_w - T_i}$$

$$\frac{\bar{V}_z}{\bar{\alpha}_t}\frac{\partial \theta}{\partial \bar{Z}} - \left(\frac{\partial^2 \theta}{\partial \bar{X}^2} + \frac{\partial^2 \theta}{\partial \bar{Z}^2}\right) + Br\left(\frac{\partial \bar{V}_z}{\partial \bar{X}}\right)^2 = 0 \tag{26}$$

where

$$Br = PrEc \quad \text{and} \quad Ec = \frac{V_0^2}{c_p(T_w - T_i)}.$$

Equation (26), cannot be solved analytically. Therefore, a numerical solution is sought by using the central finite difference method. In the present work it is assumed that both plates have constant and equal temperatures and the inlet temperature of the fluid is known. The solution obtained leads to the temperature distribution in the $X$–$Z$ plane of the channel.

### HEAT TRANSFER COEFFICIENT

According to the energy balance

$$-k_f \frac{\partial T}{\partial X}\bigg|_{X=\pm a} = h(T_w - T_m) \tag{27}$$

where

$$T_m = \frac{1}{V_{av}A_c}\int_{A_c} V_z T \, dA_c. \tag{28}$$

Non-dimensionalizing equation (27) we obtain

$$Nu = \frac{2ha}{k_f} = \frac{2}{\theta_m}\frac{\partial\theta}{\partial \bar{X}}\bigg|_{\bar{X}=\pm 1} \tag{29}$$

where

$$\theta_m = \frac{T_w - T_m}{T_w - T_i}.$$

The derivatives

$$\frac{\partial\theta}{\partial \bar{X}}\bigg|_{\bar{X}=\pm 1}$$

are calculated numerically using the standard three point formulae. Also the average Nusselt number is calculated as

$$Nu_{av} = \frac{1}{\bar{Z}}\int_0^1 Nu \, d\bar{Z}. \tag{30}$$

### RESULTS AND DISCUSSION

The mathematical model developed in the previous sections was applied to predict the fluid flow and heat transfer characteristics through a microchannel. Looking at the preceding theory, one will find that in addition to the non-dimensional electrokinetic separation distance $\kappa$, three more non-dimensional parameters, $G_1$, $G_2$ and $G_3$, also play important roles in such a microchannel flow. $\kappa = a * k$ characterizes the ratio of the distance between the two plates to the double layer thickness and is a function of both the channel size and the fluid properties. $G_1 = a^2P_z/\mu V_0$ represents the ratio of the mechanical force to viscous force. $G_2 = \xi n_0 zea^2/l\mu V_0$ represents the ratio of EDL force to viscous force. $G_3 = V_0 n_0 zel/\xi\lambda_0$ characterizes the ratio of the streaming current to conduction

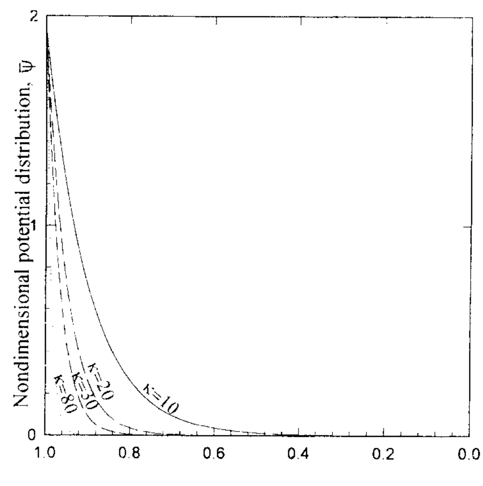


Fig. 3. Nondimensional electrostatic potential distribution near the channel wall for $\xi = 50$ mV. $\bar{X} = 0$, center of the channel and $\bar{X} = 1$, the channel wall.

current. For given values of these three non-dimensional parameters an estimation of flow and heat transfer characterizing parameters such as velocity, streaming potential, ratio $\mu_a/\mu$ and $Nu$ can be obtained.

To obtain an estimation of these parameters, consider fully developed laminar flow of an infinitely diluted ($n_0 = 6.022 \times 10^{20}$ m$^{-3}$) aqueous 1 : 1 electrolyte (e.g. KCl) solution through a microchannel. The separation distance is 25 $\mu$m and the channel is 1 cm long. At room temperature, the physical and electrical properties of the liquid are $\varepsilon = 80$, $\lambda_0 = 1.2639 \times 10^{-7}$ ($1/\Omega$m), $\mu = 0.90 \times 10^{-3}$ (kg m s$^{-1}$). A pressure difference of 4 ATM and an arbitrarily chosen reference velocity $V_0 = 1$ m s$^{-1}$ are considered. With these, a set of values $G_1 = 5.009$, $G_2 = 7.95 \times 10^{-5}$, $G_3 = 1.6 \times 10^8$ and $\kappa = 40.8$ is obtained for a fixed value of $\xi = 50$ mV. Predictions are made for velocity distribution, streaming potential, apparent viscosity and local and average Nusselt numbers.

### PREDICTION OF POTENTIAL DISTRIBUTION

Equation (6) was solved with the linear approximation for the potential distribution of the solid–liquid interfacial EDL field. The solution equation (8), gives very close values to the exact analytical solution for small electrostatic potentials at the wall. A comparison of the potential distribution based on linear approximation with the exact potential distribution can be found elsewhere, [10, 13]. The linear solution predicts slightly lower values of the potential at the wall compared to exact solution but at a small distance from the wall the two solutions overlap. The variation of non-dimensional potential distribution $\bar{\psi}$ with the nondimensional distance for various values of $\kappa$ is shown in Fig. 3. For any given electrolyte, a large $\kappa$ implies either a large separation distance

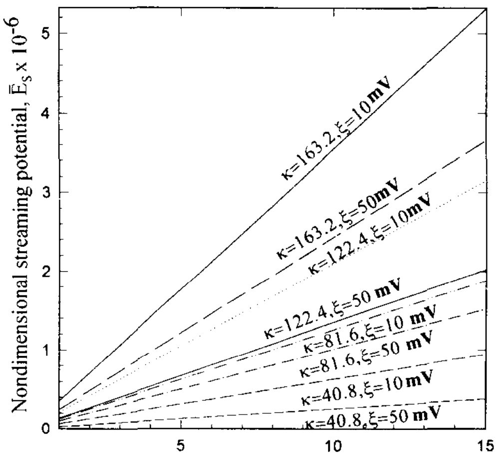


Fig. 4. Nondimensional streaming potential variation with $G_1$ for various $\kappa$ and $\xi$.

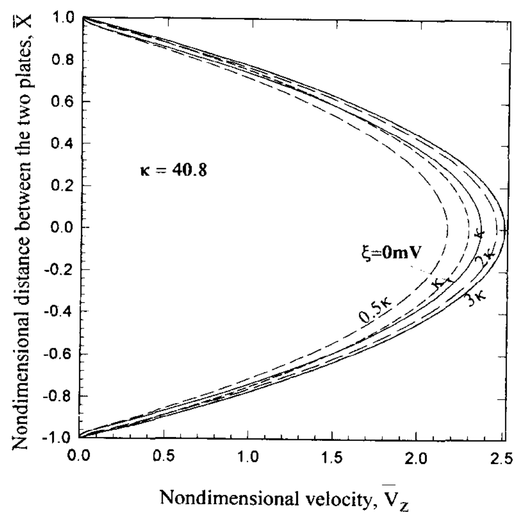


Fig. 5. Nondimensional velocity distribution for various $\kappa$ with $\xi = 50$ mV.

between the two plates or small EDL thickness. It can be seen that as $\kappa$ increases the double layer field exists only in the region close to the channel wall. For example, for $\kappa \approx 80$, the double layer occupies only 8% of the channel cross-sectional area. Therefore the smaller the $\kappa$ the more predominant is the effect of the double layer field.

## VELOCITY DISTRIBUTION AND STREAMING POTENTIAL

To obtain $\bar{V}_z$, $\bar{E}_s$ is to be determined first. This can be calculated for any given values of $G_1$, $G_2$, $G_3$, $\xi$ and $\kappa$ from equation (17). As $G_1 \propto P_z$, thus a higher pressure implies a higher $G_1$. $E_s \propto G_1$, thus the higher the pressure the higher the streaming potential. Figure 4 shows the variation of $\bar{E}_s$ with $G_1$ for various values of $\kappa$ and $\xi$. It is observed that as $G_1$ increases the streaming potential increases. Also for a given value of $\xi$, $\bar{E}_s$ increases with $\kappa$. This is because, a large electrokinetic separation distance corresponds to a large volume transport and thus more ions are carried to the end of the channel which result in higher charge accumulation. As seen from Fig. 4 as $\xi$ increases $\bar{E}_s$ decreases. This is due to the strong effect of the double layer potential of the channel wall. If the zeta potential is higher, then more ions are attracted by the oppositely charged ions in the double layer and less ions are carried to the downstream with the flow; resulting in a lower charge accumulation at the ends of the channel.

For fixed values of $G_1$, $G_2$, $G_3$ and $\xi$ the variation of velocity for different values of $\kappa$ is shown in Fig. 5. As seen, the velocity profiles are parabolic in shape and that as $\kappa$ increases the velocity increases. The reason for this is that increasing $\kappa$ implies either a large separation distance between the plates or a smaller EDL thickness resulting in larger portion of fluid not being affected by the EDL. However, if the EDL effect is absent ($\xi = 0$ mV, $\kappa$), Fig. 5 shows that the velocity is higher than when it is present ($\xi = 50$ mV, $\kappa$). Thus the EDL modifies the velocity profile which would affect the pressure drop and heat transfer.

## PREDICTIONS FOR FRICTION CONSTANT

The product of the friction factor and $Re$ as given by equation (23) was computed for various values of $\xi$. Without considering the effects of the EDL the friction constant $C_f = 24$ was given by the conventional theory, but as can be seen from Fig. 6, as $\xi$ increases $C_f$ also increases. For $\kappa = 40.8$ at $\xi = 100$ mV, the value of the $C_f = 28.22$. As $\kappa$ increases the values of $C_f$ tend towards the conventional value of 24. For $\kappa = 163.2$, the maximum value of $C_f$ at $\xi = 100$ mV is 24.1. Therefore, for small $\kappa$ the friction constant is higher depending on the zeta potential. Therefore, both the channel size and the fluid properties will affect the friction constant.

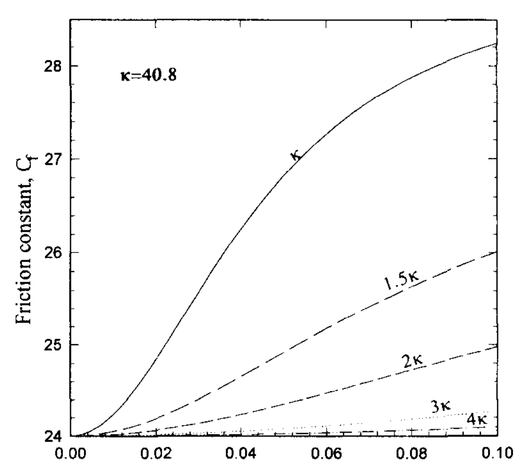


Fig. 6. Variation of $C_f$ with $\xi$ for different values of $\kappa$.

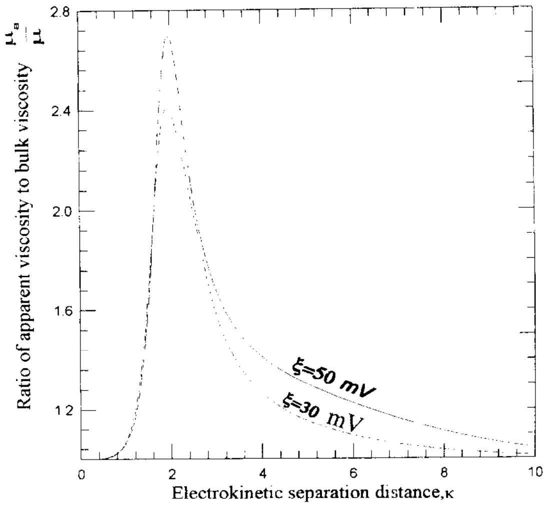


Fig. 7. Variation of the ratio of apparent viscosity to bulk viscosity with $\kappa$.

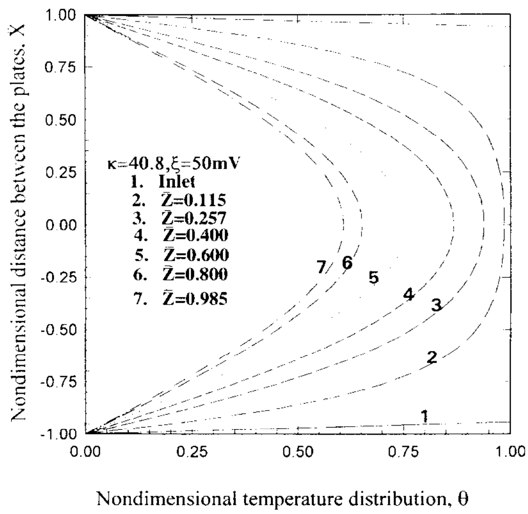


Fig. 8a. Temperature profile at various cross-sections for $Re = 2.83$.

## PREDICTIONS FOR APPARENT VISCOSITY

As explained above, the streaming potential drives ions to move opposite to the flow direction and these moving ions drag the surrounding liquid molecules with them. This generates a reduced volume flow rate as given by equation (19). Comparing this reduced volume flow rate with the flow rate derived by using conventional theory results in an apparent viscosity, which is greater than the bulk viscosity. Using equation (22) the ratio of the apparent viscosity to the bulk viscosity, $\mu_a/\mu$, is plotted as a function of $\kappa$ in Fig. 7. It is observed that for $\xi = 50$ mV, the value of the ratio is approximately 2.75 when $\kappa = 2$ and then decreases as $\kappa$ increases approaching a constant value equal to one for very large values of $\kappa$. For lower values of $\xi$ the trend is the same except the value of the ratio is lower. This pattern has also been reported by [11, 12].

## PREDICTIONS FOR HEAT TRANSFER

To predict the behavior of heat transfer in microchannels, the energy equation was solved numerically. Here, a hydrodynamically-developed and thermally-developing flow with constant and equal wall temperatures was considered. The EDL at the solid–liquid interface results in reduced velocity which directly affects the heat transfer in the channel. To analyze the heat transfer behavior in microchannels it is important to consider the effect of $Re$ on temperature profile at various cross-sections along the channel length. Figure 8(a, b), shows temperature profiles for $Re = 2.83$ and $Re = 56.5$, respectively. One can observe distinct difference in the two figures. At the entrance of the channel, marked as inlet in the figures, the temperature profiles are very steep compared to profiles at the exit. For $Re = 2.83$, the temperature profile has a parabolic shape like the fully developed velocity profile, but for $Re = 56.5$, the temperature profile resembles a turbulent velocity profile shape. A steep temperature profile at the entrance implies a higher value of the derivative $\partial\theta/\partial\bar{X}$ at $\bar{X} = \pm 1$. In addition $\theta_m$ is also maximum at the entrance of the channel. According to equation (29), $Nu$ has a maximum value at the channel entrance. Along the flow channel, both $\partial\theta/\partial\bar{X}$ at $\bar{X} = \pm 1$ and $\theta_m$ decrease. However, the value of the derivative $\partial\theta/\partial\bar{X}$ decreases much faster than $\theta_m$, which results in a lower $Nu$. This can be seen in Fig. 9, in which $Nu$ is plotted for various values of $\kappa$ and $\xi$ along the channel length. For $\kappa = 40.8$ and 163.2 if there are no double layer effects i.e. $\xi = 0$, a higher value of $Nu$, i.e. higher heat transfer rate, is obtained. For the same value of $\kappa$, $Nu$ decreases as $\xi$ increases. As $\kappa$ increases (for example, for the same

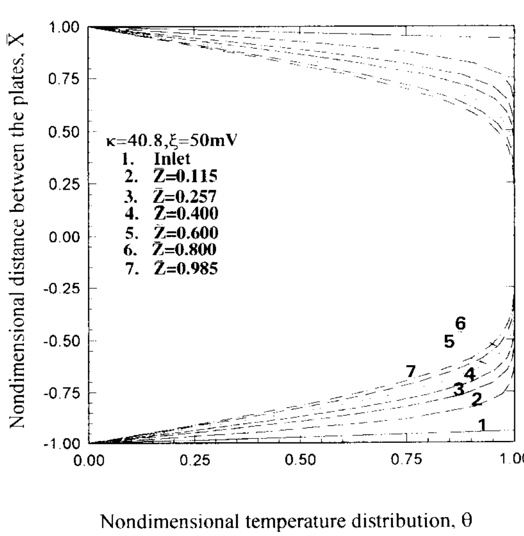


Fig. 8b. Temperature profile at various cross-sections for $Re = 56.5$.

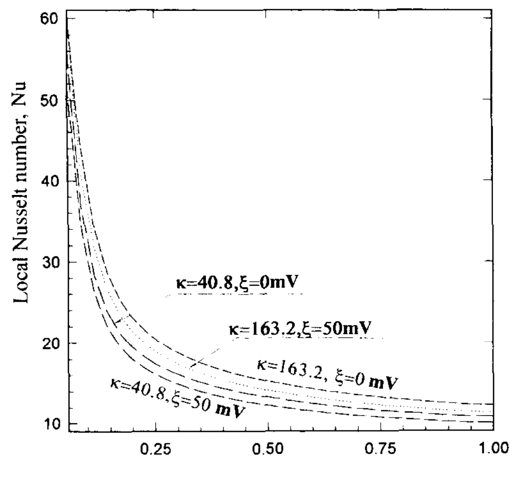


Fig. 9. Variation of local Nusselt number, $Nu$ along the channel length.

channel size with a weaker EDL field or a smaller EDL thickness), the value of $Nu$ increases as can be seen from Fig. 9. The variation of the average Nusselt number, $Nu_{av}$ as given by equation (30), with the Reynolds number, $Re$, is shown in Fig. 10. It is observed that as $Re$ increases, the $Nu_{av}$ also increases. The above predictions are in agreement with the work of [9]. They [8, 9, 14] showed experimentally that fluid properties and geometry of the microchannels all have significant influence on heat transfer performance and characteristics. As we have demonstrated in this work that the heat transfer dependence on fluid properties and on the channel's geometry may be understood as the EDL effects, as the parameters $G_2$, $G_3$ and $\kappa$ are functions of channel geometry and fluid properties. The EDL has a significant effect on $Nu$ and hence heat transfer rate. Without considering this effect we may very well overestimate the heat transfer rate in microscale channels.

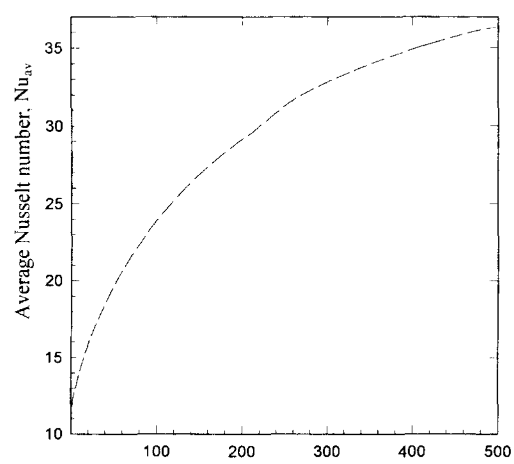


Fig. 10. Variation of the average Nusselt number, $Nu_{av}$ with Reynolds number, $Re$ for $\kappa = 40.8$ and $\xi = 50$ mV.


## SUMMARY

The effects of the EDL at the solid–liquid interface on liquid flows and heat transfer through a microchannel between two parallel plates were studied. Generally, the EDL near the channel wall tends to restrict the motion of ions and hence the liquid molecules in the diffuse EDL region. The induced streaming potential will drive the ions and hence the liquid molecules to move opposite to the flow direction. It is seen that for higher electrokinetic separation distance $\kappa$, the influence of the double layer is predominant only at the region near the channel wall. For small $\kappa$ the double layers have a significant effect on the liquid flow. The streaming potential increases with an increase in $\kappa$, while it decreases for higher surface or zeta potentials. The EDL and the streaming potential act against the liquid flow resulting in a higher apparent viscosity. The apparent viscosity can be several times higher than the bulk viscosity of the liquid when the electrokinetic separation distance $\kappa$ is very small. The heat transfer is also affected by EDL. The EDL results in a reduced velocity of flow than in conventional theory, thus affecting the temperature distribution and reducing the Reynolds number. It is seen that without the double layer a higher heat transfer rate is predicted, while as with a small zeta potential at the surface of the channel the heat transfer rate is comparatively smaller. Thus in our opinion it is very important to consider the effects of the EDL on liquid flows and heat transfer in microchannels. Otherwise, we would overestimate the fluid flow and heat transfer capacity of the system.


*Acknowledgments*—The authors wish to acknowledge the support of a University of Alberta Ph.D. Scholarship (Gh. Mohiuddin Mala) and the Natural Science and Engineering Research Council of Canada, Research Grants (D. Li and J.D. Dale).

## REFERENCES


1. Lai, J., Carrejo, J. P. and Majumdar, A., Thermal imaging and analysis at submicrometer scale using atomic force microscope. *ASME-HTD*, 1993, **253**, 13–20.
2. Tuckermann, D. B. and Pease, R. F. W., High performance heat sinks for VLSI. *IEEE Electron Device Letters*, 1981, **2**, 126–129.
3. Philips, R. J., Microchannel heat sinks. In: *Advances in Thermal Modeling of Electronic Components and Systems* (ed. A. Bar-Cohen and A.D. Kraus), Vol. II Chap. 3. ASME Press, New York, 1990.
4. Eringen, A., Simple microfluids. *International Journal of Engineering Science*, 1964, **2**, 205–217.
5. Pfahler, J. N., Liquid transport in micron and submicron channels. Ph.D. thesis, University of Pennsylvania, PA, 1992.
6. Choi, S. B., Barron, R. F. and Warrington, R. O., Fluid flow and heat transfer in microtubes. *ASME Proceedings*, 1991, **32**, 123–134.

7. Harley, J. and Bau, H., Fluid flow in micron and submicron size channels. *IEEE Transactions THO*, 1989, **249-3,** 25–28.
8. Peng, X. F., Peterson, G. P. and Wang, B. X., Heat transfer characteristics of water flowing through microchannels. *Experimental Heat Transfer*, 1994, **7,** 265–283.
9. Wang, B. X. and Peng, X. F., Experimental investigation on liquid forced convection heat transfer through microchannels. *International Journal of Heat and Mass Transfer*, 1994, **37**(Suppl. 1), 73–82.
10. Hunter, R. J., *Zeta Potential in Colloid Science: Principles and Applications*. Academic Press, New York, 1981.
11. Rice, C. L. and Whitehead, R., Electrokinetic flow in narrow cylindrical capillaries. *Journal of Physical Chemistry*, 1965, **69,** 4017–4023.
12. Levine, S., Marriott, J. R., Neale, G. and Epstein, N., Theory of electrokinetic flow in fine cylindrical capillaries at high zeta potential. *Journal of Colloid Science*, 1975, **52,** 136–149.
13. Adamson, A. W. *Physical Chemistry of Surfaces*. John Wiley, New York, 1990.
14. Peng, X. F., Wang, B. X., Peterson, G. P. and Ma, H. B., Experimental investigation of heat transfer in flat plates with rectangular microchannels. *International Journal of Heat and Mass Transfer*, 1995, **38,** 127–137.